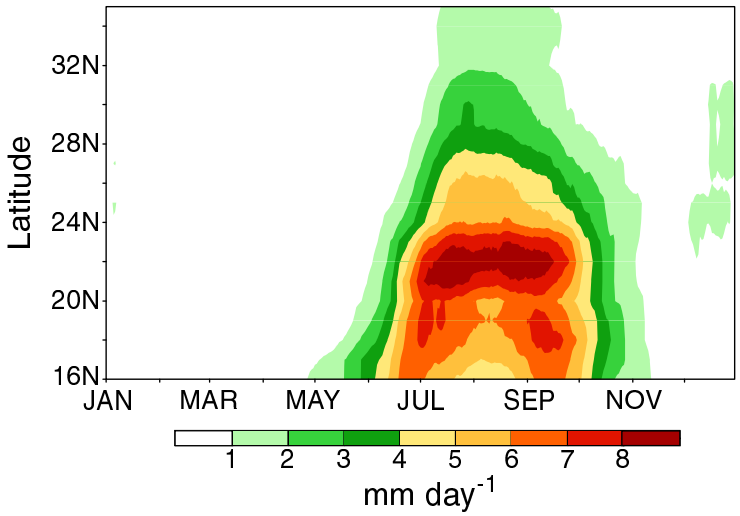

Figure 10. Time-latitude sections of the mean (1961-1990) annual cycle of precipitation. Data are averaged zonally over west coast land points at each latitude.

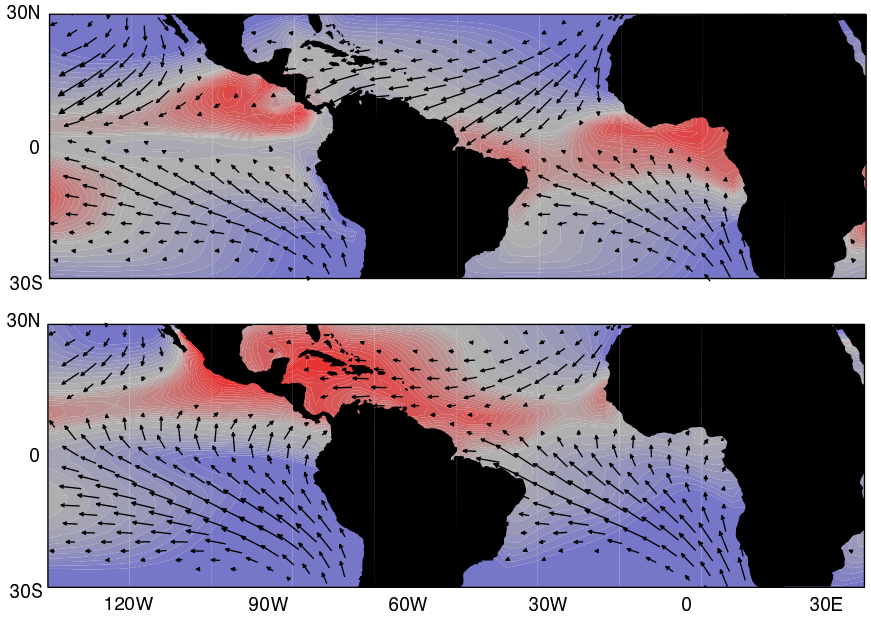

Figure 11. As in Fig. 3 but for the March-April mean (upper panel) and September-October mean conditions (lower panel). The warm pool to the north of the equator is present year round. The largest seasonal contrasts are observed along the southern flank of the equatorial cold tongue. September-October is the time of strongest meridional temperature contrast across the equator.

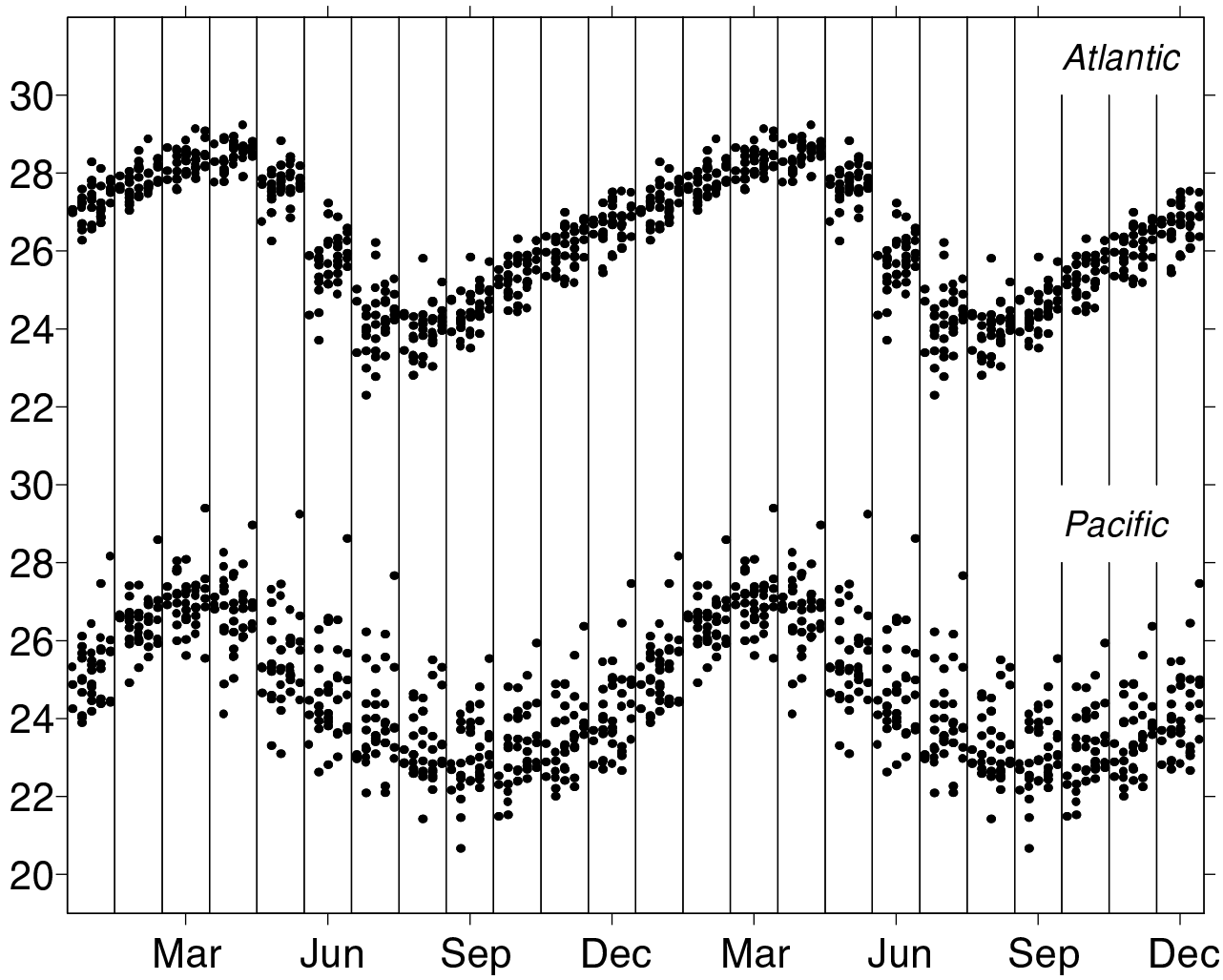

Figure 12. Scatter plot of monthly mean sea surface temperature (°C) in the equatorial cold tongue regions of the Atlantic and Pacific for individual years/months, grouped by calendar month. The dots for each calendar month are staggered along the *x* axis to make them more visible, and the calendar year is repeated. Note the high degree of reproducibility of the seasonal march, particularly in the Atlantic, where El Niño exerts only a modest influence.

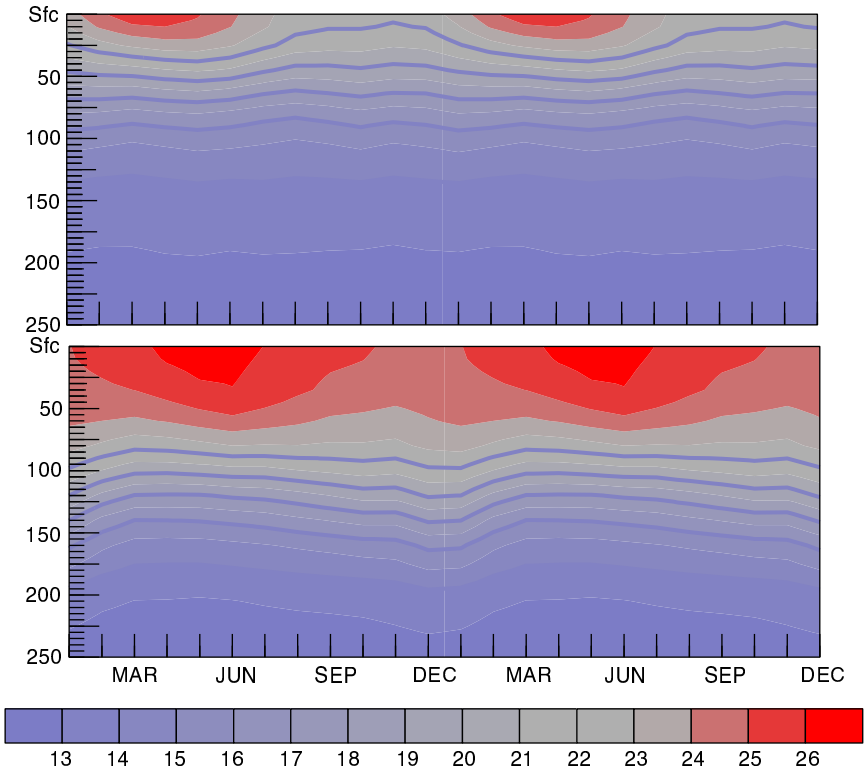

Figure 13. Depth-time sections of climatological mean temperature (°C) on the equator at 110°W (upper panel) and 140°W (lower panel) showing how the seasonal march tends to be much stronger near the surface than near the thermocline.

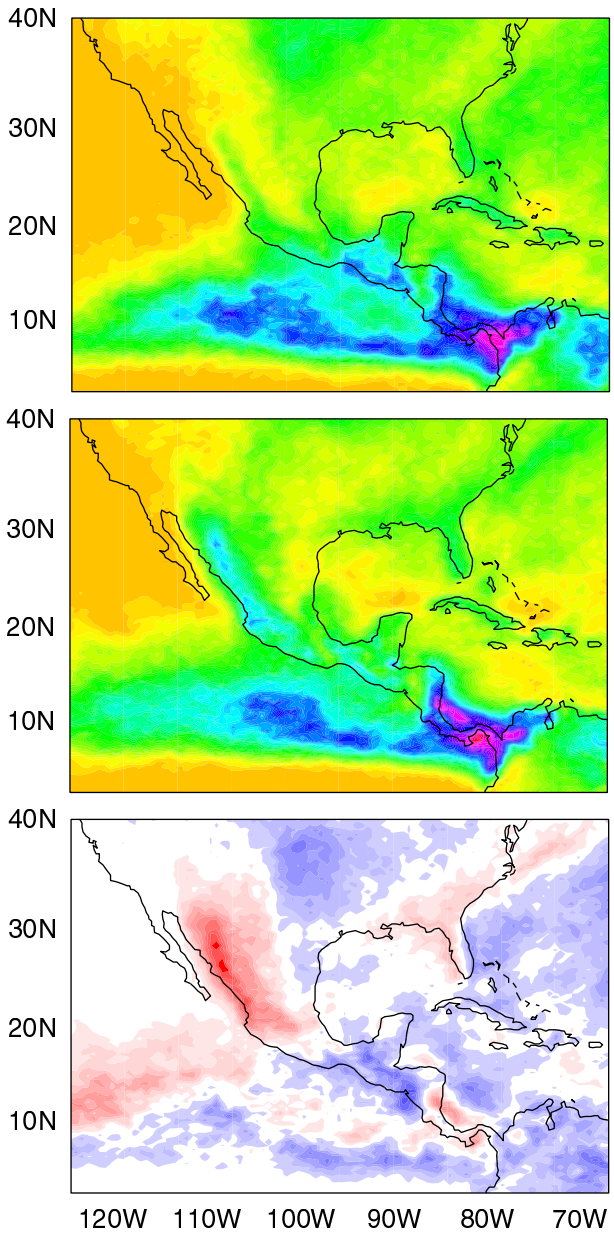

Figure 14. Frequency of occurrence of clouds with tops colder than -38°C as revealed by high-resolution satellite imagery for the years 1990-93. (top) June, (middle) July, (bottom) the difference of July minus June. In most years, the northward shift of the rainfall in northwestern Mexico and Arizona occurs rather abruptly around July 1. Despite this shift, the same distinctive signature of the orography and coastal geometry is evident during both months over much of Central America.

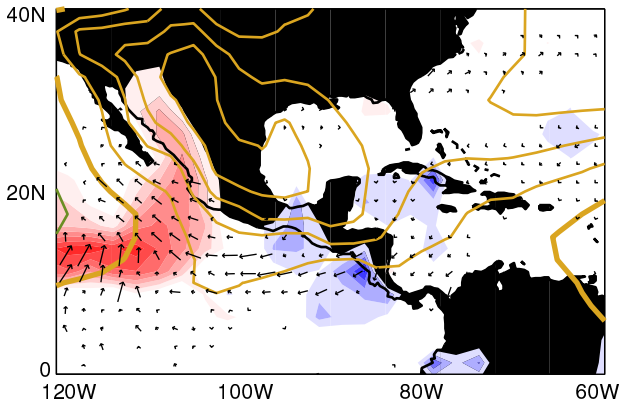

Figure 15. July minus June differences in surface winds (arrows), sea-level pressure (contours: gold denotes pressure increases; zero contour thickened), and rainfall (shading: red denotes increases and blue decreases). The freshening of the trades over much of Central America is related to the rise in sea-level pressure over Mexico. The prevailing northwesterly winds along the west coast of Mexico weaken, allowing surges of moist southerly flow to penetrate into the Gulf of California. The linkage between month-to-month changes in the continental monsoon and the ITCZ appears to be stronger in the microwave sounding unit imagery and rain gauge data shown here than in the infrared imagery shown in the previous figure.

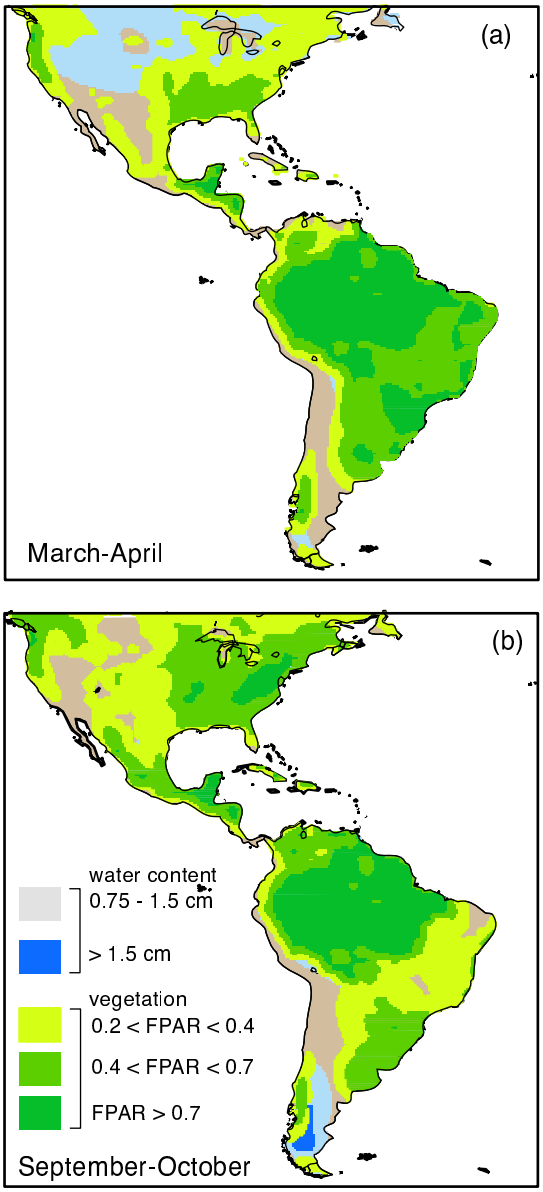

Figure 16. March-April mean (upper panel) and September - October mean (lower panel) soil moisture and vegetation (FPAR). Soil moisture and FPAR as in Fig. 7.

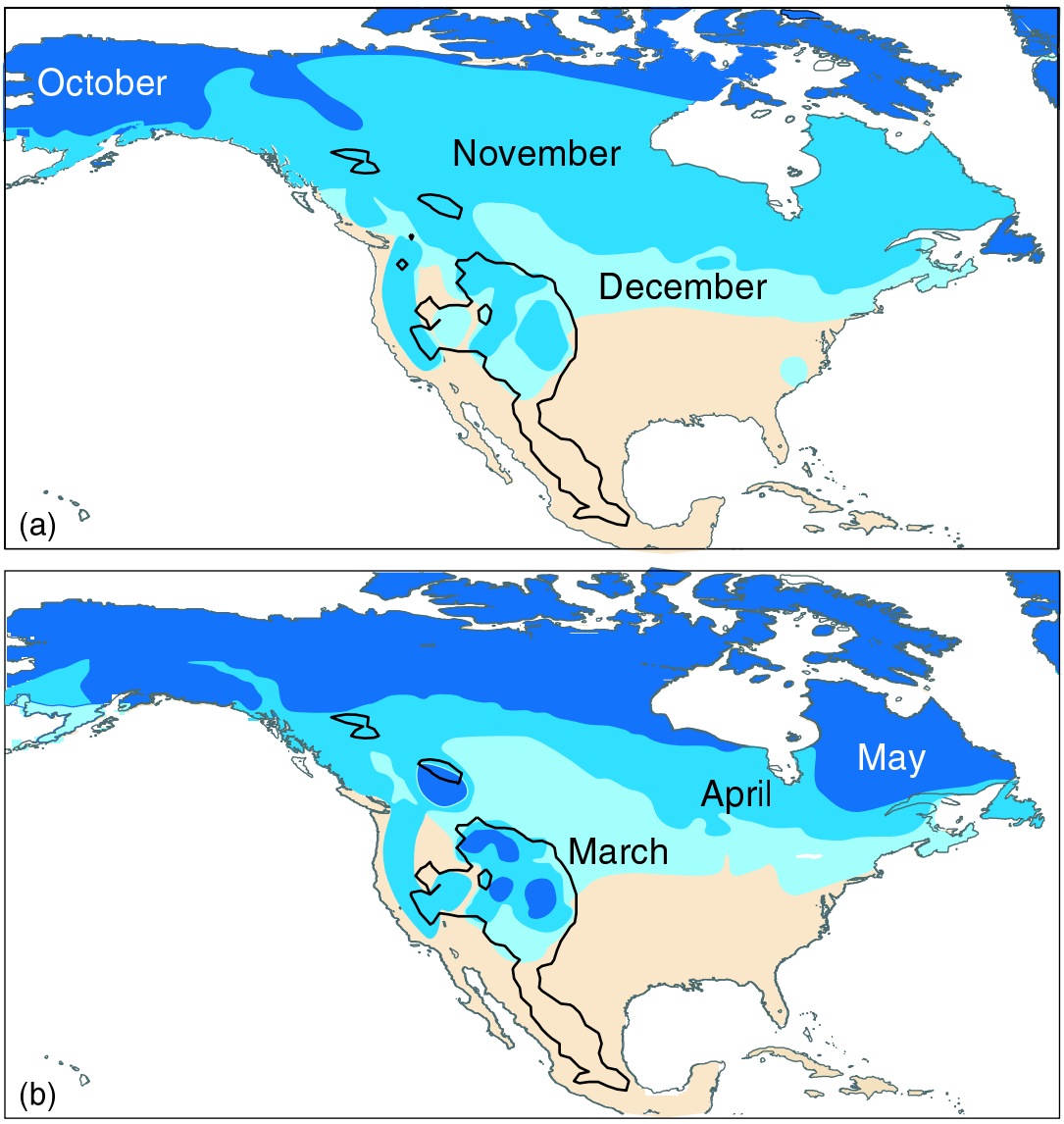

Figure 17. Seasonal march of the snow line at (a) the beginning and (b) end of Northern Hemisphere winter. Darker blues indicate cooler temperatures. Elevation contour is 1500 m.

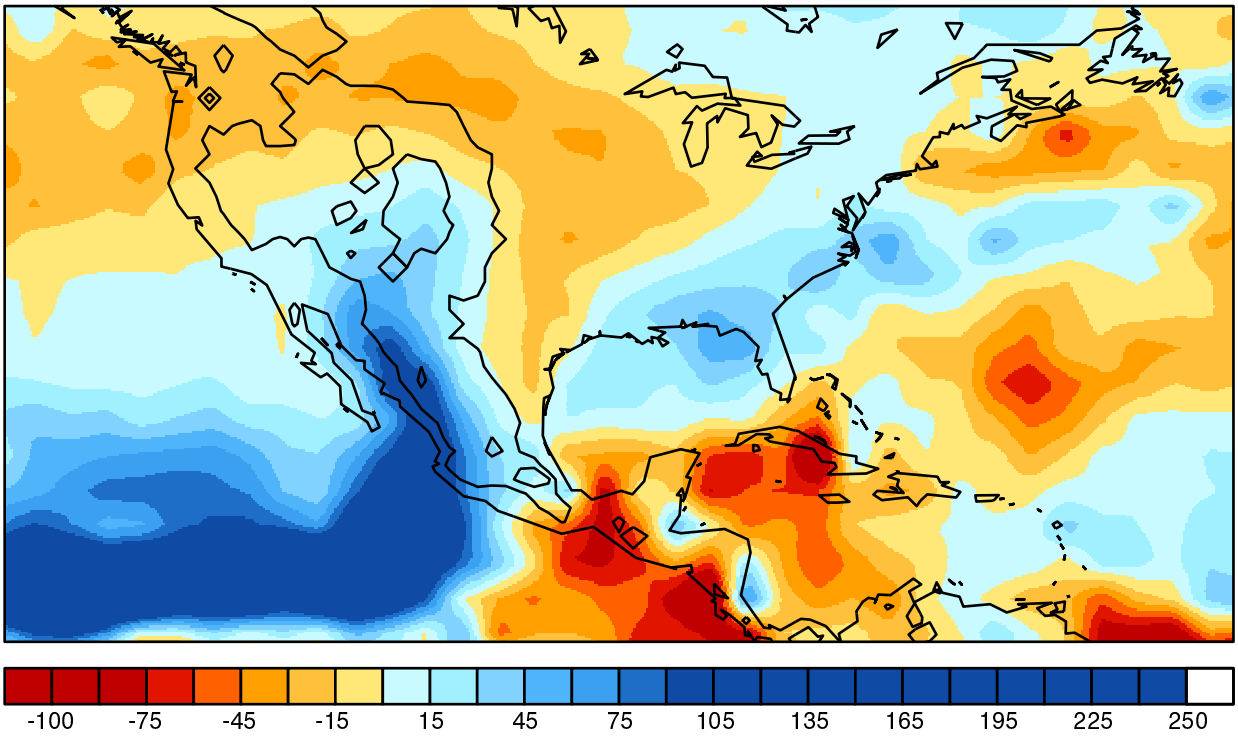

Figure 18. Climatological mean July minus June precipitation (mm/month).

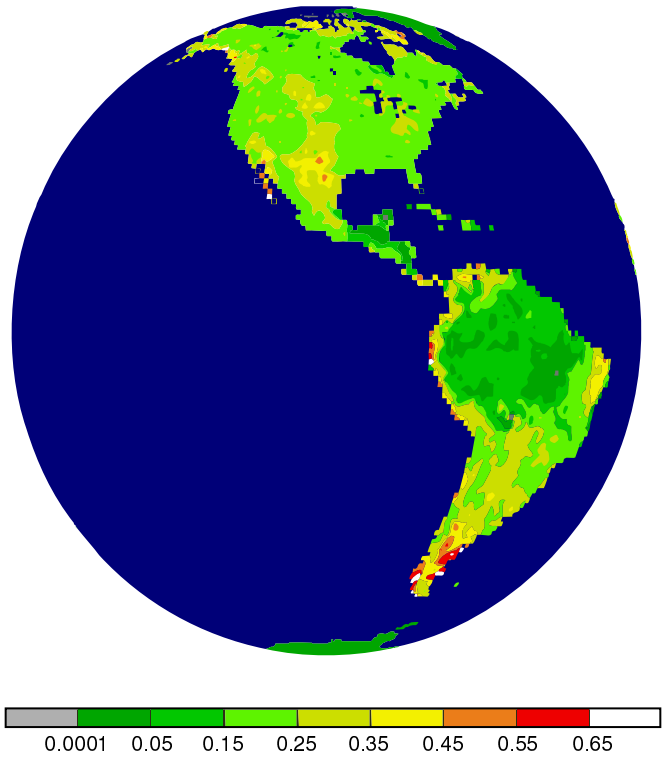

Figure 19. Interannual variability of leaf area index (LAI). The index is the ratio of the one-half of the leaf area to the area of the ground surface.